Mechanism, energetics, kinetics and dynamics of the reaction $C_2H_6^{+\cdot} \rightarrow C_2H_4^{+\cdot} + H_2$

ARTICLE *in* JOURNAL OF MASS SPECTROMETRY · OCTOBER 1993

Impact Factor: 2.38 · DOI: 10.1002/oms.1210281043

ORGANIC MASS SPECTROMETRY, VOL. 28, 1262–1269 (1993)

Mechanism, Energetics, Kinetics and Dynamics of the Reaction $C_2H_6^{+\bullet} \rightarrow C_2H_4^{+\bullet} + H_2$

Svein Magne Bråten, Trygve Helgaker and Einar Uggerud
Department of Chemistry, University of Oslo, P.O. Box 1033 Blindern, N-0315 Oslo, Norway

Tore Vulpius
Department of Chemistry, H. C. Ørsted Institute, University of Copenhagen, DK-2100 Copenhagen, Denmark

The distributions of relative translational energy released during (i) loss of H_2 from metastable $CH_3CH_3^{+\bullet}$ ions, (ii) loss of HD from metastable $CH_3CD_3^{+\bullet}$ ions and (iii) loss of D_2 from metastable $CD_3CD_3^{+\bullet}$ ions were measured. The relevant parts of the potential energy surface of the reaction $C_2H_6^{+\bullet} \rightarrow C_2H_4^{+\bullet} + H_2$ (including isotopic variants) were investigated using various theoretical methods (high-level *ab initio* quantum chemistry, RRKM calculations, dynamic reaction trajectory calculations). A consistent reaction model is presented which reproduces available experimental data. Quantum mechanical barrier tunnelling is found to be important, leading to an activation energy (on the microsecond time-scale) which is approximately 0.1 eV below the critical energy.

INTRODUCTION

Dehydrogenation and hydrogenation reactions play a central role in organic chemistry.[1] Ethylene, which is important intermediate for the production of ethanol and polyethylene, is produced industrially by the gas-phase pyrolysis of ethane.[2] The reaction

$$CH_3CH_3 \rightarrow CH_2CH_2 + H_2 \qquad (1)$$

is known not to occur via direct unimolecular elimination of H_2. Instead, a multi-step radical mechanism is followed. This mechanism involves initial homolytic cleavage of the C—C bond of ethane. The direct pathway (1,2-elimination) is avoided as the result of an extraordinarily high energy barrier. Quantum chemical calculations by Gordon *et al.*[3] indicated a critical energy of 512 kJ mol^{-1}. The bond dissociation energy of the C—C bond in ethane is known to be 367 kJ mol^{-1}. To make the unimolecular 1,2-elimination kinetically more feasible, a catalyst may be used. Commonly used catalysts for hydrogenation and dehydrogenation include transition metals bonded in various forms.

Several transition metal ions are known to promote direct H_2 elimination. This has been demonstrated in mass spectrometric experiments.[4] Among factors that seem to be essential for the activity of a metal is the availability of empty 4s orbitals for electron acceptance.[3,5] An interesting situation occurs when one electron has been removed from ethane, as in $CH_3CH_3^{+\bullet}$. The activation energy for dehydrogenation of the ethane cation is 56 kJ mol^{-1} (see below), only 11% of the corresponding quantity of reaction (1).

Using electron impact ionization, the appearance energy for the formation of $C_2H_4^{+\bullet}$ from C_2H_6 was measured as early as in 1938 by Hipple[6] to be 12.2 eV [ionization enegy IE(ethane) = 11.52 eV].[7] In 1946, Hipple *et al.*[8] demonstrated that metastable $C_2H_6^{+\bullet}$ ions lose H_2 during flight through a magnet sector mass spectrometer. This observation gave support to the idea that an intact H_2 molecule rather than two H atoms are lost. By performing a series of charge-exchange reactions with ethane, Lindholm[9a] and von Koch[9b] showed in 1965 that at the energetic threshold HD (and not H_2 or D_2) is exclusively lost from $CH_3CD_3^{+\bullet}$. This is a strong indication of a concerted 1,2,-dihydrogen elimination mechanism. Photoionization[10] and photoelectron–photoion coincidence (PEPICO) measurements[11] have been reported. From these measurements a value for the activation energy of E_a = 56 kJ mol^{-1} and of the reverse activation energy of E_a^r = 25 kJ mol^{-1} are obtained.[11c] A TPEPICO value of E_a = 64 kJ mol^{-1} has recently been reported.[11d]

The first measurement of the translational energy release was made by Taubert[12] in 1964, giving T = 0.45 eV. Improved measurements by Lifshitz and Sternberg[13] gave $T_{0.5}$ = 0.20 eV and $T_{0.5}$ = 0.10 eV for reactions (2) and (4), respectively.

$$CH_3CH_3^{+\bullet} \rightarrow CH_2CH_2^{+\bullet} + HH \qquad (2)$$

$$CH_3CD_3^{+\bullet} \rightarrow CH_2CD_2^{+\bullet} + HD \qquad (3)$$

$$CD_3CD_3^{+\bullet} \rightarrow CD_2CD_2^{+\bullet} + DD \qquad (4)$$

In 1974, Williams and Hvistendahl reported $T_{0.5}$ = 0.19 eV.[14] Williams and Hvistendahl suggested that the reaction is symmetry forbidden (Woodward–Hoffmann rules) owing to the large fraction of the reverse activation energy (T/E_a^r) which is released in the form of relative translation of the products. A symmetric transition state was inferred from their analysis. MINDO/3 calculations by Dewar and Rzepa[15] indicated a 'skewed' transition state. This means that the H_2 elimination is concerted, but that one of the hydrogens approaches one hydrogen of the other carbon so that the H_2 entity formed departs in an unsymmetrical fashion.

0030–493X/93/101262–08 $09.00

Received 25 May 1993
Revised manuscript received 29 June 1993
Accepted 30 June 1993

The purpose of this paper is to provide a consistent model of reaction (2). Energetic, kinetic and dynamic factors will be addressed. New high-resolution experimental data on the translational energy release distribution of reactions (2)–(4) provide a check of the calculated dynamic model.

EXPERIMENTAL

Measurements of translational energy release were made using two instruments, a two-sector (EB geometry, $V_0 = 6$ or 7 kV) mass spectrometer (MS 902, AEI Instruments) and a four-sector (EBEB geometry, $V_0 = 10$ kV) mass spectrometer (JMS-HX/HX110 A, Jeol). To obtain first field-free region metastable ion decomposition profiles from the two-sector instrument, the V-scan method[16] was employed. With the four-sector instrument, the reactant ion was selected using the two first sectors. Decompositions occurring in the third field-free region were then recorded by scanning the second E sector [mass-analysed ion kinetic energy (MIKE) scan].[17] Intermediate energy-defining slits were set narrow to obtain the highest possible energy resolution, which for both instruments is better than 0.1%. To arrive at translational energy release distribution functions free from instrumental effects, the metastable peak profiles were analysed using the method of Rumpf and Derrick.[18] Samples of ethane and ethane-d_6 were purchased from AGA Norgas and Cambridge Isotope Laboratories, respectively. CD_3CH_3 was synthesized by reaction of CH_3Li with CD_3Br in a glass-lined apparatus.[19] Capillary column (CSQ, 30 m × 0.53 mm i.d.; J&W Scientific) gas–liquid chromatography/mass spectrometry was employed to verify the chemical and isotopic purity of the samples.

THEORETICAL MODEL

Quantum chemical calculations were done using the program systems GAUSSIAN 92[20] and SIRIUS/ABACUS.[21] Two different basis sets were used, the medium-sized (M) basis 4–31G(d,p) and the large (L) basis 6–311 + G(2dp,2df). The latter basis set consists of a split valence (311) plus two sets of two polarization functions plus diffuse p-functions for carbon. This basis set gives 152 basis functions with 190 primitive gaussians. The quantum chemical methods used were restricted Hartree–Fock (RHF), unrestricted Hartree–Fock (UHF), Möller–Plesset perturbation theory to second-(MP2) and fourth-order excitations (MP4) and quadratic configuration interaction with single and double excitations (QCISD). Geometry optimizations were performed for the reactant, transition structure and products at all levels of theory employed except MP4/L, for which the optimized UHF/L geometries were used. The Hessian (second-derivative matrix) was calculated and checked for the correct number of eigenvalues. The vibrational frequencies used in calculating the zero-point energies and the RRKM calculations were taken from the UHF/M results after scaling with a factor[22] of 0.9. The geometric parameters reported are from the QCISD/M calculations. The methods used for the RRKM and dynamic reaction path calculations will be described in more detail in the sections where the results are reported and discussed.

REACTION MECHANISM AND ENERGETICS

At all levels of theory the reactant molecule $C_2H_6^{+\cdot}$ (*a*) was calculated to have a structure of the type shown in Fig. 1. The optimized QCISD/4–31G(d,p) geometry shows that the central C—C bond distance is 1.927 Å, which is almost 0.4 Å longer than for neutral C_2H_6. The methyl groups are staggered as in neutral C_2H_6. The small H—C—C angle of 98° indicates an approximate sp^2 hybridization around the two carbon atoms. These findings are in agreement with earlier calculations.[23] We conclude that ionization of ethane occurs from an MO with a strong σC—C bond character. The large geometry distortion on ionization is also reflected in an essentially zero Franck–Condon factor for the $0 \rightarrow 0$ transition observed in the photoelectron spectrum of ethane.[24] The weakness of the C—C bond in *a* is also reflected in calculated [HF/4–31(d,p)] stretching frequency of ν_{str}(C–C) = 413 cm^{-1}, which should be compared with ν_{str}(C–C) around 1280 cm^{-1} in neutral ethane (calculated using data from Ref. 25). Removal of an electron also has dramatic consequences for the C—C and C—H bond strengths. The bond dissociation

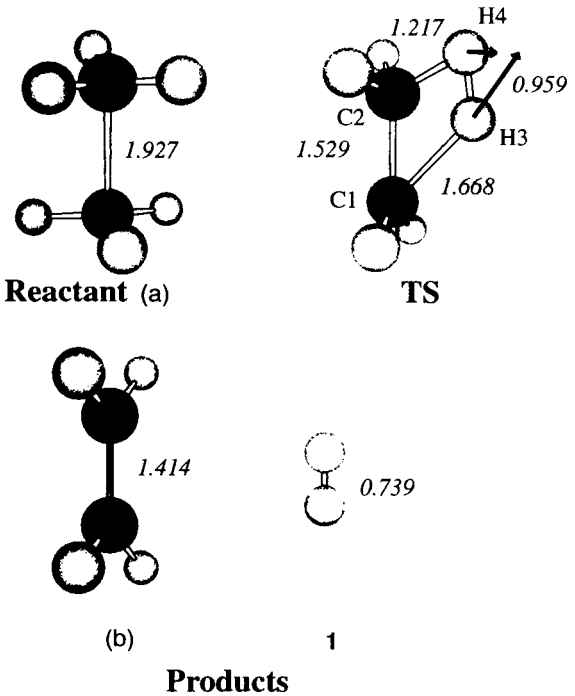

Figure 1. Optimized molecular geometries of reactant, transition structure (TS) and products obtained by QCISD/4–31G(d,p). Only the most important bond distances (in Å) are indicated. The most prominent components of the reaction coordinate (mass dependent) have been included for the TS geometry.

energies for the processes

$$CH_3CH_3^{+\cdot} \rightarrow CH_3^+ + CH_3^{\cdot} \quad (5)$$

$$CH_3CH_3^{+\cdot} \rightarrow C_2H_5^+ + H^{\cdot} \quad (6)$$

have been measured by PEPICO to be 207 and 88 kJ mol^{-1}, respectively.[11c] These values should be compared with the well established values of 367 and 414 kJ mol^{-1} for the homolytic C—C bond and C—H bond dissociation energies in ethane at 0 K.[7]

The flexibility of the ethane cation is also reflected in the modest energy requirement for the transition structure (TS) of reaction (2), as can be seen from Table 1. The TS is in good agreement with the experimentally established 1,2-elimination mechanism (Fig. 1). The reaction is not symmetrical, however, since the two H atoms [H(3) and H(4)] do not depart along an axis perpendicular to the mid-point of the C—C bond. Instead, the C(1)—H(3) bond is stretched far more than the C(2)—H(4) bond, so that the reaction centre is tilted towards and above C(2). The lengths of the C—H bonds and the H(3)—H(4) distance of only 0.959 Å clearly indicate a tight transition state. This is in perfect agreement with the TPEPICO results.[11d] Analysis of the reaction coordinate ($\nu = i1027$ cm^{-1}) shows that the largest components are those of H(3) and H(4) as shown in Fig. 1. The reaction coordinate is thus in complete agreement with a concerted mechanism. As we have demonstrated by a dynamic calculation (see below), this TS leads directly to the expected products, $C_2H_4^{+\cdot}$ (*b*) and H_2 (**1**). A reviewer has put forward the problem that the H_2 moiety of the transition structure could be 'floppy', i.e. the two hydrogens rotate easily relative to the C—C bond. The calculations reveal that this is not the case. The harmonic analysis shows that the indicated motion correponds to a torsional vibration with $\nu = 674$ cm^{-1}.

The energy difference between reactant and products is known experimentally to be $\Delta E = 31$ kJ mol^{-1} (Table 1). With RHF or UHF this quantity is poorly reproduced, as is seen from Table 1. There is little improvement in going from the medium-sized basis 4–31G(d,p) to the large basis 6–311 + G(2df,2dp). Dynamic electron correlation improves the situation as shown by the MP2/4–31G(d,p) and QCISD/4–31G(d,p) results. Both a large basis set and correlation are needed for quantitative agreement with experiment, in accord with previous calculations on similar reactions.[26] At the MP4/6–311 + G(2df,2pd) level of theory the calculated energy difference is $\Delta E = 29$ kJ mol^{-1}.

The calculated critical energy for the reaction, E_c (the energy difference between TS and reactant, see Fig. 2) also depends strongly on the method used. Again the UHF and RHF values are seen to deviate significantly from the experimental activation energy of $E_a = 56$ kJ mol^{-1}, whereas the MP4/6–311 + G(2df,2dp) result with $E_c = 58$ kJ mol^{-1} is only 2 kJ mol^{-1} higher than experiment. The MP2 and QCISD calculations also give satisfactory results. It therefore seems that dynamic electron correlation is sufficient in order to describe the potential energy surface of the reaction.

This is surprising since 1,2-H_2 eliminations have been described[14,27] as forbidden according to the Woodward–Hoffmann (W–H) reaction symmetry rules.[28] A symmetrical concerted four-electron/four-centre reaction (as in the hypothetical symmetrical hydrogenation of ethylene) leads to orbital near degeneracy in the TS. One would therefore expect that a proper description of the orbital crossing would have to take static electron correlation explicitly into account, e.g. by using multi-configurational (MC) SCF wavefunctions.

To investigate the importance of such static electron correlation effects, we carried out MCSCF calculations

Table 1. Energy data from *ab initio* calculations[a]

Energy	$CH_3CH_3^{+\cdot}$ (*a*)	Transition structure (TS)	Products (*b* + **1**)	$CH_2CH_2^{+\cdot}$ (*b*)	H_2 (**1**)
E(RHF/M)	−78.781 89	−78.732 51	−78.772 12	−77.640 79	−1.131 33
E(UHF/M)	−78.785 06	−78.737 20	−78.774 14	−77.642 81	−1.131 33
E(UHF/L)	−78.883 87	−78.837 34	−78.872 35	−77.739 35	−1.133 00
E(MP2/M)	−79.054 48	−79.028 68	−79.037 96	−77.880 30	−1.157 66
E(QCISD/M)	−79.084 55	−79.051 72	−79.067 86	−77.903 29	−1.164 57
E(MP4/L)	−79.242 38	−79.216 96	−79.221 67	−78.050 00	−1.171 67
E(zpv)	174.5	165.4	148.9	124.0	24.9
Δ*E*(RHF/M)	0	121	0		
Δ*E*(UHF/M)	0	117	3		
Δ*E*(UHF/L)	0	113	5		
Δ*E*(MP2/M)	0	59	18		
Δ*E*(QCISD/M)	0	77	18		
Δ*E*(MP4/L)	0	58	29		
$\Delta\Delta H_0$(exp.)	0	56	31		

[a] Absolute energies (*E*) are given in hartree and zero-point vibrational energies [*E*(zpv)] and energy differences (Δ*E*) in kJ mol^{-1}. All calculated energy differences are obtained by inclusion of zero-point vibrational energies. Calculations were done with the 4–31G(d,p) (M) or 6–311 + G(2df,2pd) (L) basis sets at geometry-optimized structures, excepts for the MP4/L calculation, where the geometry from the UHF/L calculation was used. Zero-point vibrational energies were obtained from the UHF/M frequencies after scaling with the factor 0.9. Experimental heat of formation data were taken from Refs 11c and 7 and are 0 K values.

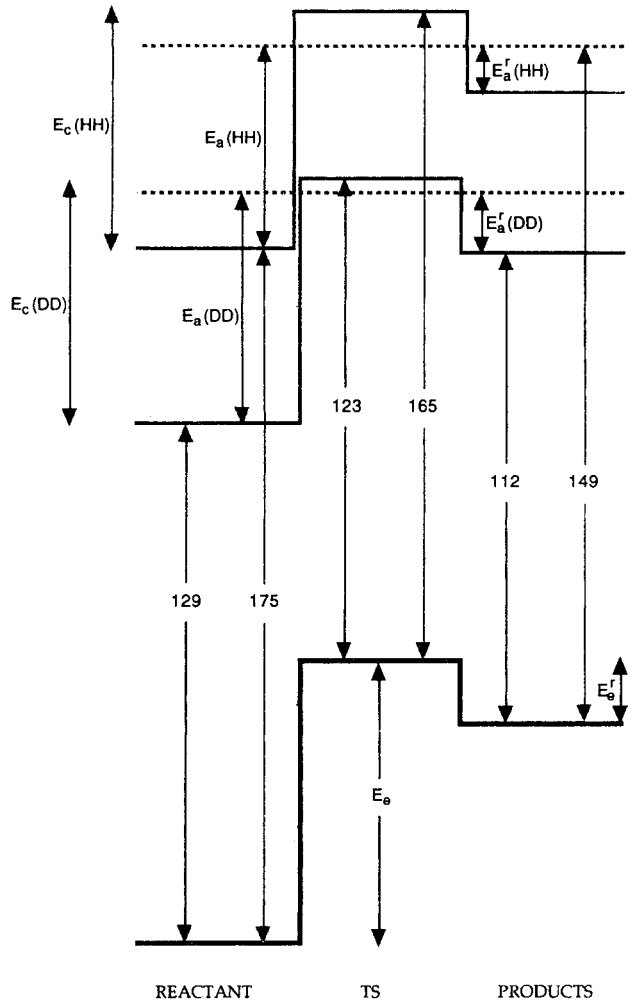

Figure 2. Schematic potential diagram of reactions (2) and (4). The thick solid line at the bottom corresponds to the electron energy levels and is the same for all isotopic reactions. The barrier heights for the forward and reverse reactions (E_e and E_e^r, respectively) are indicated. Addition of zero-point vibrational energies (numbers given are in kJ mol^{-1}) result in molecular potential energy levels for reaction (2) (HH, upper thin solid line) and for reaction (4) (DD, lower thin solid line). The critical energy for a reaction (E_c) is the molecular potential energy difference between the TS and the reactant, and the reverse critical energy (E_c^r) is the molecular potential energy difference between the TS and the fragments. Since vibrational frequencies are different for isotopic species, values for E_c and E_c^r are in general different for isotopic reactions. Also shown are the activation energies for the forward and the reverse reactions (E_a and E_a^r). The values of these quantities are obtained from appearance energy measurements and depend on instrumental and physical factors as discussed in the text.

of the transition structure and for the fragmented species. For example, in a complete active space (CAS) MCSCF calculation obtained by distributing 13 electrons among 12 active orbitals, no near degeneracy effects were observed, all occupations being within 0.030 of 2, 1 or 0 at the TS and within 0.022 for the fragmented system. We conclude that the correlation effects are all dynamic and best described by single-configuration based methods.

The reason for this may be that the reaction under investigation does not strictly fulfil the requirements for being 'forbidden' by the W–H rules because it is an open electron shell molecular system. Another important point is that the calculations show that the TS is not symmetrical as required in the W–H formalism. In fact, symmetrical H_2 eliminations do not appear to be very common. To our knowledge, no truly symmetrical H_2 eliminations have yet been reported, even in closed electron systems. Both the TS for H_2 loss from ethane[3] and the TS for H_2 loss from protonated formaldehyde[29] have, for example, been demonstrated to have non-symmetrical structures. In both cases the reactions seem to be well described at the MP level of theory.

REACTION KINETICS, RRKM CALCULATIONS

The appearance energy of a reaction measured in a particular mass spectrometric experiment depends on the time between ion formation and decomposition, Δt. It has been noted that as Δt becomes longer, the lower is the appearance energy and therefore the observed activation energy. This phenomenon can be explained by taking the kinetics of the unimolecular reaction into account. Because the rate generally increases with increasing internal energy, the high-energy part of the reactant ion population is gradually depleted as Δt increases. The difference between the observed activation energy and the 'true' critical energy is usually termed the kinetic shift.[30] In order to be able to compare the *ab initio* critical energy reported here with the PEPICO activation energy,[11c] we decided to calculate the energy dependence of the rate coefficients of reactions (2)–(4). For this purpose the RRKM theory was employed.

The procedure used to calculate the rate coefficient $k(E)$ has been described by Miller.[31] The expression used is

$$k(E) = \frac{\sum P^*(E - E_c)}{hP(E)} \tag{7}$$

where $P(E)$ and $P^*(E - E_c)$ are the quantum mechanical densities of state for the reacting molecule and the transition state, respectively, and h is Planck's constant. The total energy is given by E and the critical energy by E_c. The summation sign in the numerator implies that for a particular value of the energy the calculated densities are integrated up to this energy. The reaction coordinate is assumed to be separable from all other internal degrees of freedom at the transition structure. Quantum mechanical tunnelling along the reaction coordinate is accounted for by using an inverted parabola potential,[28] requiring only the imaginary frequency as input to the computer program. For a given total energy and kinetic energy the tunnelling probability in the reaction coordinate (both below and above E_c) was calculated before integration was performed. Since the reaction has a tight transition state, rotational degrees of freedom were excluded.[32] The vibrational energy densities were obtained numerically by the Beyer–Swinehart algorithm[33] using the *ab initio* vibrational frequencies scaled by a factor of 0.9 (Table 2).

RRKM calculations were carried out for three different values, E_c = 58, 68 and 78 kJ mol^{-1}; the first value

Table 2. *Ab initio* frequencies (scaled by 0.9) used in the RRKM calculations

Reaction	TS frequencies (cm^{-1})	Reactant frequencies (cm^{-1})
$C_2H_6^{+\cdot} \rightarrow C_2H_4^{+\cdot} + H_2$	1027*i* 305, 531, 674, 809, 920, 957 1144, 1361, 1382, 1392, 1451, 2274, 2336, 2940, 2998, 3039, 3137	195, 413, 577, 579, 629, 631, 1201, 1254, 1375, 1377, 1387, 1389, 2912, 2920, 3078, 3080, 388, 3090
$CH_3CD_3^{+\cdot} \rightarrow CH_2CHD_2^{+\cdot} + HD$	785*i* 243, 410, 570, 749, 772, 896, 1035, 1048, 1315, 1382, 1430, 1677, 2164, 2310, 2349, 2936, 3039	169, 399, 439, 441, 603, 605, 938, 1015, 1017, 1228, 1380, 1382, 2067, 2299, 2301, 2915, 3083, 3085
$CD_3CH_3^{+\cdot} \rightarrow CD_2CH_2^{+\cdot} + DH$	999*i* 278, 529, 560, 691, 809, 811, 1019, 1045, 1086, 1108, 1393, 1721, 2083, 2270, 2311, 2998, 3137	169, 399, 439, 441, 603, 605, 938, 1015, 1017, 1228, 1380, 1382, 2067, 2299, 2301, 2915, 3083, 3085
$C_2D_6^{+\cdot} \rightarrow C_2D_4^{+\cdot} + D_2$	764*i* 216, 408, 482, 679, 692, 780, 895, 980, 1011, 1025, 1080, 1644, 1690, 2135, 2165, 2270, 2349	138, 385, 428, 430, 445, 447, 429, 948, 1008, 1010, 1021, 1023, 2064, 2069, 2294, 2296, 2303, 2305

corresponds to the best (MP4/L) *ab initio* value. The rate curves are reproduced in Fig. 3. A direct comparison with the PEPICO data[11c] is difficult because the time-scale (Δt) of the experiment was not given. Typical reaction times are of the order of 1 μs. We therefore assumed that $k = 10^6$ s^{-1} leads to representative values of the activation energies as indicated in Fig. 3. The activation energies energy corresponding to the three E_c values are then estimated to $E_a = 38$, 52 and 64 kJ mol^{-1}. In all cases there is a substantial negative kinetic shift due to tunnelling. The magnitude of the shift is largest for the smallest E_c value. By interpolation it can be found that the PEPIDO E_a value of 56 kJ mol^{-1} approximately corresponds to an E_c value between 71 and 73 kJ mol^{-1}.

Keeping the uncertainty of Δt and the RRKM approximations in mind, it seems that the best *ab initio* value for the critical energy may be too low by ~12–14 kJ mol^{-1}, which is still satisfactory because the quoted uncertainty of the PEPICO E_a value is ±10 kJ mol^{-1}. Despite these uncertainties, it is clear from the RRKM calculations that tunnelling does occur and should be taken into account in understanding the dissociation dynamics of the reactions. It should be mentioned that if the TPEPICO value of E_a is used instead of the PEPICO value, all quantities deduced from the above analysis shift by 8 kJ mol^{-1}.

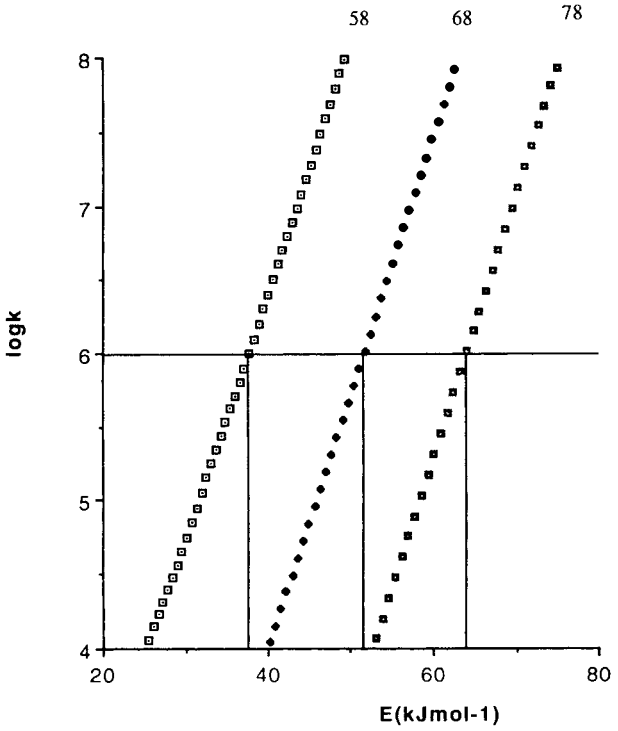

Figure 3. Rate curves obtained from RRKM calculations for three different values of E_c. For reactions which have $k(E) = 10^6$ s^{-1} the energies (which correspond roughly to the activation energy, E_a) are indicated.

Figure 2 shows that isotopic substitution affects the zero-point energies of the molecular species differently, and thereby the values of E_c and E_c^r. In addition, the kinetics are affected because vibrational energy level densities and tunnelling probabilities change. A series of RRKM calculations was therefore conducted for the isotopic reactions (2)–(4). In the case of reaction (3) two different transition structures may lead to elimination of the elements of H and D, in reaction (3a) the hydrogens of C(1) have been replaced with deuterium (this gives HD loss) and in reaction (3b) the hydrogens of C(2) have been replaced with deuterium (which gives DH loss). The resulting decrease in reaction path degeneracy was accounted for in the calculation of the rate coefficients. A value of the critical energy of $E_c = 73$ kJ mol^{-1} was chosen for reaction (2) in accordance with the findings reported above. After correction for differences in zero-point energies (Fig. 2), this leads to the critical energies of the three other isotopic reactions given in Table 3. The vibrational frequencies used are given in Table 2 and the rate curves in Fig. 4.

A comparison of the curves for HH and DD [reactions (2) and (4)] reveals that the rate of the former reaction is higher by about two orders of magnitude at all energies. The curve for DD is also steeper below E_c. This leads to a much smaller negative kinetic shift in the case of DD, as would be expected from the much smaller probability for barrier tunnelling. A similar analysis to that used above (using $k = 10^6$ s^{-1}) shows that the activation energy for DD is 71 kJ mol^{-1} compared with 57 kJ mol^{-1} for HH. This is also illustrated in Fig. 2. The curves for HD and DH lie between those for HH and DD. Compared with the HD curve, the DH curve is closest to that of HH because of both the smaller value for E_c and the higher tunnelling probability. The higher tunnelling probability stems from the fact that movement of H(3) (which in this case is an H

Table 3. Energy data (kJ mol^{-1} unless stated otherwise) for the isotopic reactions (all quantities are defined in the text)

Reaction	Departing molecule	Zero-point vibrational energies [E(zpv)] Reactant	TS	Products	Critical energies for forward and reverse reactions E_c	E_c^r	Estimated activation energies for forward and reverse reactions E_a	E_a^r	Translational energies from dynamic calculations T_{calc} (hartree)	T_{rel} (T_{calc} as % of E_c^r)
(2)	HH	174.5	165.4	148.9	73	42	57	26	0.0385	85.3
(3a)	HD	151.7	145.5	131.0	76	40	68	32	0.0398	85.6
(3b)	DH	151.7	142.7	131.0	73	37	62	26	0.0338	84.1
(4)	DD	128.9	122.7	112.0	76	36	71	31	0.0341	85.9

and not a D atom) has the largest component of the reaction coordinate. The results of this analysis are given in Table 3.

TRANSLATIONAL ENERGY RELEASE AND REACTION DYNAMICS

As explained in the experimental section, translational energy releases were measured using two different instruments. Figure 5 shows the metastable peak profile obtained for reaction (2) by scanning[16] of the ion source potential (V) of the EB instrument. The corresponding translational energy release distribution function is reproduced in Fig. 6 together with the distributions for reactions (3) and (4). The translational energy release distribution for reaction (2) obtained by MIKE scanning of the second E sector of the EBEB instrument is shown in Fig. 7. Only relative minor differences in the distribution function can be observed. The V-scan distribution has a T_{mp} (most probable value for T) of 0.16 eV, whereas in the MIKE-scan distribution it is 0.18 eV. The widths are approximately the same. In the case of the V-scan distribution a small hump on the low-energy tail is noticed. This may be an artifact due to the incomplete basis functions used in the deconvolution of the instrument function. The observed T_{mp} values are close to the previous $T_{0.5}$ values given in the Introduction. A value of $T_{mp} = 0.18$ eV corresponds to 67% of $E_a^r = 26$ kJ mol^{-1} (Table 3). This percentage is, of course, somewhat arbitrary taking into account the experimental uncertainty of ± 10 kJ mol^{-1} in the case of E_a^r. An isotope effect is observed (V-scan) for reactions (3) and (4), with $T_{mp} = 0.18$ and 0.20 eV, respectively.

The translational energy release distribution function of a unimolecular reaction is determined by several factors, the most important of which are the form of the internal energy distributions of the decomposing ions and the detailed dynamics of the reaction path followed by each individual ion. In previous papers[34] we have demonstrated that representative values for translational energy release can be reproduced by integration of the classical equations of motion. A representative path (which corresponds to a molecule which reacts at its energetic threshold) starts at the TS and ends up with the separated products. In this treatment the force field at each point of the reaction path is calculated *ab initio*. This integration has become feasible as the result of an efficient algorithm developed and implemented by us.[34a]

Dynamic calculations of representative paths for the four reactions (2)–(4) were performed following the procedure previously described.[34b] The wavefunction used in the calculation was the RHF/M described above. A larger calculation could not be performed because more than 100 points along the path (including analytical first and second derivatives in the molecular energy) are required for each molecular system.

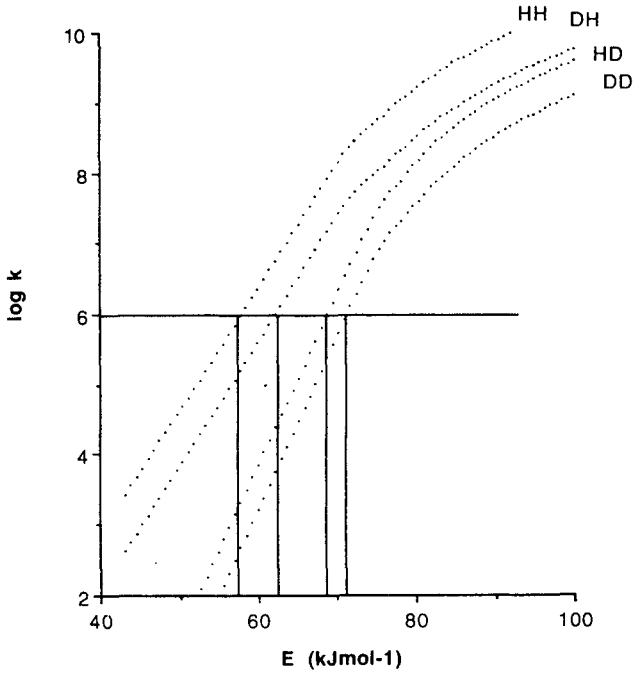

Figure 4. Rate curves obtained from RRKM calculations for the four isotopic reactions.

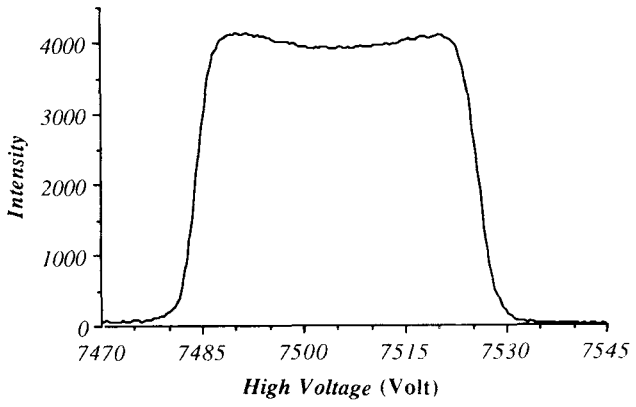

Figure 5. Metastable peak profile for $CH_3CH_3^{+\cdot} \rightarrow CH_3CH_3^{+\cdot} + H_2$ obtained by V-scanning ($V_0 = 7000$ V).

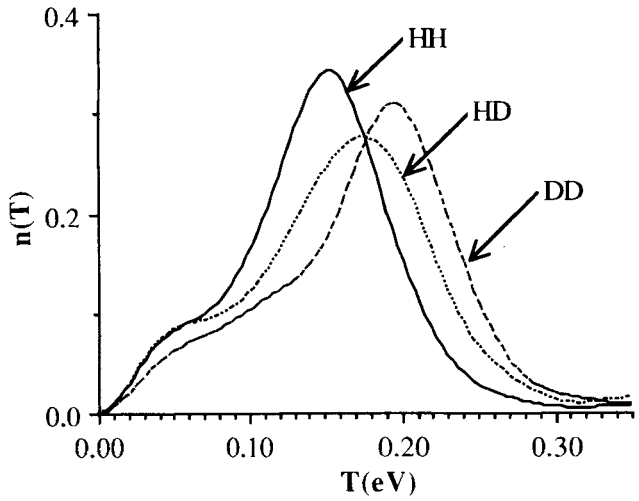

Figure 6. Distributions of translational energy release for loss of H_2 from metastable $CH_3CH_3^{+\cdot}$ ions, loss of HD from metastable $CH_3CD_3^{+\cdot}$ ions and loss of D_2 from metastable $CD_3CD_3^{+\cdot}$ (from *V*-scanning).

The calculated reaction path for reaction (2) is reproduced in Fig. 8. Although the method reproduces the barrier height poorly, the relative amount of the reverse potential energy barrier which is liberated in the form of relative translational energy is reasonably well reproduced. Since the approach is purely classical (zero-point vibrations are neglected), the energy barrier, E_e^r = 104 kJ mol^{-1}, is the same for all isotopic reactions. The results for the four isotopic reactions are given in Table 2.

This classical approach fails to reproduce the observed isotope effect on translational energy release. With hindsight this is reasonable. The reason is probably that quantum effects are so prominent in this case. As noted in the previous section, quantum mechanical barrier tunnelling leads to different values for the reverse activation energies (Table 3). The estimated value of E_a^r for reaction (2) is only 83% of that of reaction (4). This is in good agreement with a T_{mp} value for reaction (2) which is about 80% of that of reaction (4) when it is assumed that the same relative proportion of E_a^r is liberated as relative translational energy in both cases, as observed in the trajectory calculations. Reaction (3) is seen to be a superposition of two distinct processes, loss of HD and DH. The former has kinetic and energetic features which are closest to reaction (4), whereas the latter has kinetic and energetic features which are closest to reaction (2). For this reason it seems reasonable that the translational energy release is somewhere between the two.

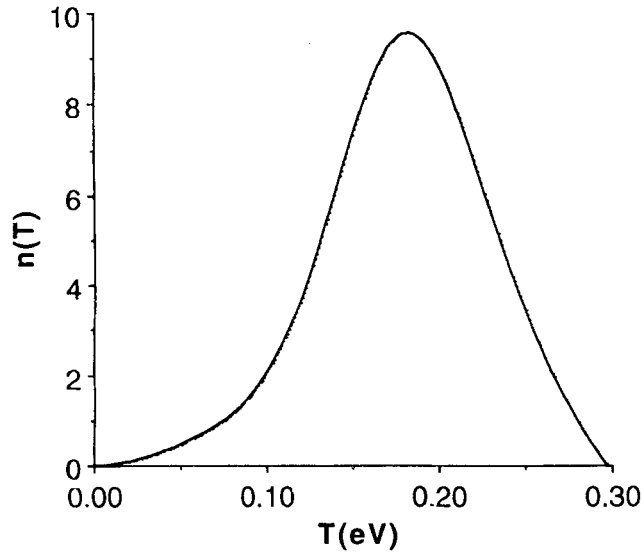

Figure 7. Distribution of translational energy release for loss of H_2 from metastable $CH_3CH_3^{+\cdot}$ ions (from MIKE scan).

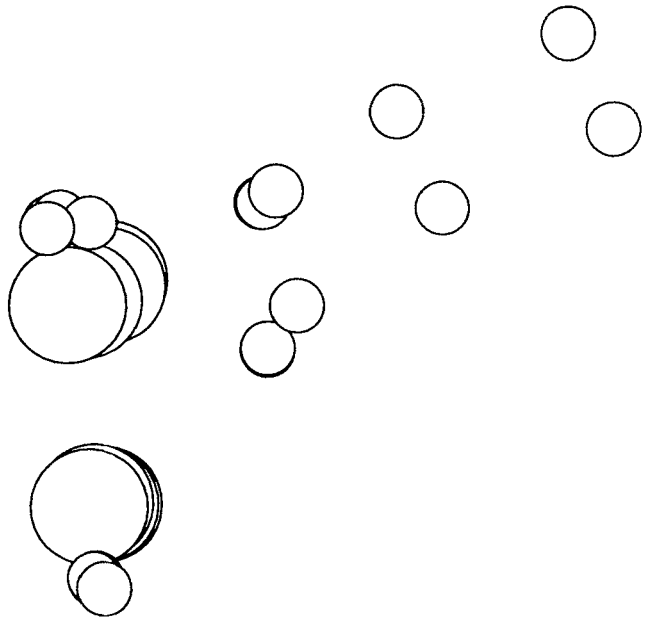

Figure 8. Illustration of the *ab initio* reaction trajectory. The picture was constructed by superimposing five snapshots of the situation at five selected points along the trajectory starting at the TS. The perspective is approximately the same as in Fig. 2. A video film has been made which animates the whole trajectory.

CONCLUSION

Our study of the H_2 elimination from $C_2H_6^{+\cdot}$ confirms that this reaction proceeds in a concerted manner via a transition structure that is non-symmetrical with respect to the two carbon atoms (the symmetrical elimination being symmetry forbidden). The barrier is low, and quantum mechanical effects such as zero-point vibrations and tunnelling are essential for a quantitative understanding of the reactions, strongly influencing rate coefficients, active barriers and translational energy releases.

Acknowledgements

E.U. expresses his personal gratitude to Professor John L. Holmes, who through his creative and thorough work on structures, thermochemistry and reactions of organic ions has proved insight and inspiration. The authors thank VISTA (the Norwegian Academy for Science and Letters and Statoil) for generous financial support and NAVF (the Norwegian Research Council) for computer time.

REFERENCES

1. See, for example, (a) H. House, *Modern Synthetic Reactions*, 2nd edn, Chapt. 1. Benjamin, Menlo Park, CA (1972); (b) P. N. Rylander, *Hydrogenation Methods*. Academic Press, New York (1985).
2. L. Kniel, O. Winter and K. Stork, *Ethylene, Keystone to the Petrochemical Industry*. Marcel Dekker, New York (1980).
3. M. S. Gordon, T. N. Truong and J. A. Pople, *Chem. Phys. Lett.* **130**, 245 (1986).
4. Reviews: (a) P. B. Armentrout and J. L. Beauchamp, *Acc. Chem. Res.* **22**, 315 (1979); (b) K. Eller and H. Schwarz, *Chem. Rev.* **91**, 1121 (1991).
5. H. Chen, D. Ekeberg, H.-Y. Lin, D. P. Ridge, K. Sohlberg and E. Uggerud, *Organometallics* submitted for publication.
6. J. A. Hipple, *Phys. Rev.* **53**, 530 (1938).
7. S. G. Lias, J. E. Bartmess, J. F. Liebman, J. L. Holmes, R. D. Levin and W. G. Mallard, *J. Phys. Chem. Ref. Data* **17**, Suppl. 1 (1988).
8. J. A. Hipple, R. E. Fox and E. U. Condon, *Phys. Rev.* **69**, 347 (1946).
9. (a) Method: E. Lindholm, *Arkiv. Fys.* **8**, 257 (1954); (b) Measurement: H. von Koch, *Arkiv. Fys.* **28**, 559 (1964).
10. W. A. Chupka and J. Berkowitz, *J. Chem. Phys.* **47**, 2921 (1967).
11. (a) E. von Puttkammer, *Z. Naturforsch., Teil A* **25**, 1062 (1970); (b) R. Stockbauer, *J. Chem. Phys.* **58**, 3800 (1973); (c) R. Bombach, J. Dannacher and J.-P. Stadelmann, *Int. J. Mass Spectrom. Ion Processes* **58**, 217 (1984); (d) K.-M. Weitzel, J. Mähnert and H. Baumgärtel, *Ber. Bunsenges. Phys. Chem.* **97**, 134 (1993).
12. R. Taubert, *Z. Naturforsch, Teil A* **19**, 911 (1964).
13. C. Lifshitz and R. Sternberg, *Int. J. Mass Spectrom. Ion Phys.* **2**, 303 (1969).
14. D. H. Williams and G. Hvistendahl, *J. Am. Chem. Soc.* **96**, 6753 (1974).
15. M. J. S. Dewar and H. S. Rzepa, *J. Am. Chem. Soc.* **99**, 7432 (1977).
16. (a) M. Barber and R. M. Elliot, paper presented at the 12th ACMS, Montreal (1964); (b) K. R. Jennings, *J. Chem. Phys.* **43**, 4176 (1965).
17. J. H. Beynon and R. G. Cooks, *Res. Dev.* **22**, 26 (1971).
18. B. A. Rumpf and P. J. Derrick, *Int. J. Mass Spectrom. Ion Processes* **82**, 239 (1988).
19. S. M. Bråten, Cand. Sci. Thesis, Department of Chemistry, University of Oslo (1992).
20. M. J. Frisch, G. W. Trucks, M. Head-Gordon, P. M. W. Gill, M. W. Wong, J. B. Foresman, B. G. Johnson, H. B. Schlegel, M. A. Robb, E. S. Replogle, R. Gomperts, J. L. Andres, K. Raghavachari, J. S. Binkley, C. Gonzalez, R. L. Martin, D. J. Fox, D. J. Defrees, J. Baker, J. J. P. Stewart and J. A. Pople, *GAUSSIAN 92*, Gaussian, Pittsburgh, PA (1992); further references to basis sets and quantum chemical procedures are given in the *GAUSSIAN 92 User's Guide*.
21. (a) H. J. Aa. Jensen and H. Ågren, *Chem. Phys.* **104**, 229 (1986); (b) T. U. Helgaker, J. Almlöf, H. J. Aa. Jenson and P. Jørgensen, *J. Chem. Phys.* **84**, 6266 (1986).
22. (a) J. A. Pople, H. B. Schlegel, R. Krishnan, D. J. DeFrees, J. S. Binkley, M. J. Frisch, R. A. Whiteside, R. F. Hout and W. J. Hehre, *Int. J. Quantum Chem. Symp.* **15**, 269 (1981); (b) G. Fogarasi and P. Pulay, *Annu. Rev. Phys. Chem.* 191 (1984).
23. (a) D. J. Bellville and N. L. Bauld, *J. Am. Chem. Soc.* **104**, 5700 (1982); (b) T. Clark, *J. Am. Chem. Soc.* **110**, 1672 (1988).
24. K. Kimura, S. Katsumata, Y. Achiba, T. Yamazaki and S. Iwata, *Handbook of He I Photoelectron Spectra of Fundamental Organic Molecules*. Japan Scientific Societies Press, Tokyo (1981).
25. A. Fadini and F.-M. Schnepel, *Vibrational Spectroscopy. Methods and Applications*. Ellis Horwood, Chichester (1989).
26. J. E. Del Bene, D. H. Aue and I. Shavitt, *J. Am. Chem. Soc.* **114**, 1631 (1992).
27. G. Hvistendahl and D. H. Williams, *J. Chem. Soc., Perkin Trans 2* 881 (1975).
28. R. B. Woodward and R. Hoffmann, *The Conservation of Orbital Symmetry*. Verlag Chemie, Weinheim (1970).
29. G. Hvistendahl and E. Uggerud, *Org. Mass Spectrom.* **26**, 67 (1991).
30. (a) Review: J. L. Holmes, *Org. Mass Spectrom.* **20**, 169 (1985); (b) Y. Malinovich and C. Lifshitz, *J. Phys. Chem.* **90**, 2200 (1986).
31. W. H. Miller, *J. Am. Chem. Soc.* **101**, 6810 (1979).
32. W. Forst, *Theory of Unimolecular Reactions*. Academic Press, New York (1973).
33. T. Beyer and D. F. Swinehart, *ACM Commun.* **16**, 379 (1973).
34. (a) T. Helgaker, E. Uggerud and H.-J. Aa. Jensen, *Chem. Phys. Lett.* **173**, 145 (1990); (b) E. Uggerud and T. Helgaker, *J. Am. Chem. Soc.* **114**, 4265 (1992).